COMPARISONS OF MEASURED AND CALCULATED POTENTIAL MAGNETIC FIELDS

M. J. HAGYARD and D. TEUBER

Space Sciences Laboratory, NASA-Marshall Space Flight Center, Marshall Space Flight Center, Ala. 35812, U.S.A.

(Received 19 December, 1977; in revised form 15 February, 1978)

Abstract. Photospheric line-of-sight and transverse magnetic field data obtained with the Marshall Space Flight Center vector magnetograph system for an isolated sunspot are described. A study of the linear polarization patterns and of the calculated transverse field lines indicates that the magnetic field of the region is very nearly potential. The Hα fibril structures of this region as seen in high resolution photographs corroborate this conclusion. Consequently, a potential field calculation is described using the measured line-of-sight fields together with assumed Neumann boundary conditions; both are necessary and sufficient for a unique solution. The computed transverse fields are then compared with the measured transverse fields to verify the potential field model and assumed boundary values. The implications of these comparisons on the validity of magnetic field extrapolations using potential theory are discussed.

1. Introduction

As a result of Skylab/Apollo Telescope Mount observations of the transition region and corona, there has been widespread interest in correlating the morphological structures seen in these data with the assumed coronal magnetic field configurations. Because coronal magnetic field measurements usually are not available, extrapolated magnetic fields are calculated using measured photospheric fields as the boundary conditions for an assumed mathematical model of the magnetic fields. One such model is the potential field which is derived from the assumption that there are no electric currents within the spatial domain of the calculation. In such a case the magnetic field at any interior point can be determined from the boundary conditions alone. Practical applications of potential theory using measured photospheric line-of-sight (longitudinal) magnetic fields as these boundary conditions include the programs of Schmidt (1964), Altschuler and Newkirk (1969) and Teuber *et al.* (1977).

A usually ignored 'by-product' of such theoretical calculations is the transverse field at the lower boundary (i.e., photosphere) which together with the measured longitudinal field comprises the vector potential field at that boundary. With the initiation of measurements of linearly polarized intensity distributions with the Marshall Space Flight Center's (MSFC) magnetograph system in 1976, the opportunity was created for making direct comparisons between the measured and computed transverse fields. On 24 November 1976, calibrated digital data were obtained on the longitudinal and transverse magnetic fields of a large, isolated

Solar Physics **57** (1978) 267–278.

sunspot (Boulder Number 757) near disk center. From these data and high resolution Hα photographs it was determined that the field morphology was very nearly potential, and thus the data provided an opportunity to make such a direct comparison. In the following sections of this paper we will describe the analysis of the sunspot data, outline the potential field calculation, and present the results of the comparison and a discussion of their implications.

2. Observational Data

The basic observational data obtained with the MSFC magnetograph system are depicted in Figure 1. To obtain the net circularly polarized intensity distributions shown in Figure 1a, the system's Zeiss birefringent filter is tuned so that the peak transmission occurs at $\approx$60 mÅ in the blue wing of the Fe I 5250.22 Å absorption line. Usually the filter is operated in the $\frac{1}{8}$ Å bandpass mode; however, for the observational data analyzed in this paper, the filter was operated at a $\frac{1}{4}$ Å bandpass, which explains the relatively weak circular polarization signals. In the measurements of the linearly polarized intensities the filter is tuned to the center of the λ 5250.22 line in order to minimize the possibility of circular signals appearing in the linear measurements ('cross-talk'); Figure 1c indicates the level of intensity of the residual circular polarization at the 'center' of the spectral line. (Since the Zeiss filter can be tuned only in steps of 10 mÅ, it is rarely possible to tune the filter to the exact central wavelength between the two σ components of the Zeeman triplet.) At line center two measurements of linearly polarized intensities are made with the planes of linear polarization oriented at 0° and 45° to the analyzer; these two measurements are shown in Figures 1d and 1e, respectively. The analyzer itself is oriented at an angle of 20° counterclockwise from the vertical direction in Figure 1. The white light intensity distribution of the sunspot is indicated in Figure 1b; the field of view of this image is 2.5×2.5 arc min, as it is for all the images in Figure 1.

In a recent paper of Hagyard *et al.* (1977), distributions of linearly polarized intensities which resembled 'pinwheels' were interpreted on the basis of a spiral configuration of the transverse magnetic field of the sunspot; the data shown in Figure 2 of that paper are representative of such pinwheel patterns. In the referenced paper it was shown that a spiral transverse magnetic field with a varying angle of spiral τ, defined in Figure 2, could reproduce the observed pattern. If τ were constant, the linearly polarized intensities would have distributions similar to those shown in Figure 3 which correspond to the case (constant) $\tau = 0°$ (a radial or potential transverse field configuration); for a nonzero, constant τ, the patterns are merely rotated by the angle τ relative to the analyzer axis. In studying the data for the sunspot discussed in this paper (region 757), it was determined that the observed linear polarization patterns more nearly resemble those of Figure 3. However, these data were not sufficient to allow us to discriminate between the case of a potential field (constant $\tau = 0°$) and a nonpotential one (constant $\tau \neq 0°$). In order to make this determination, transverse field lines were plotted from the

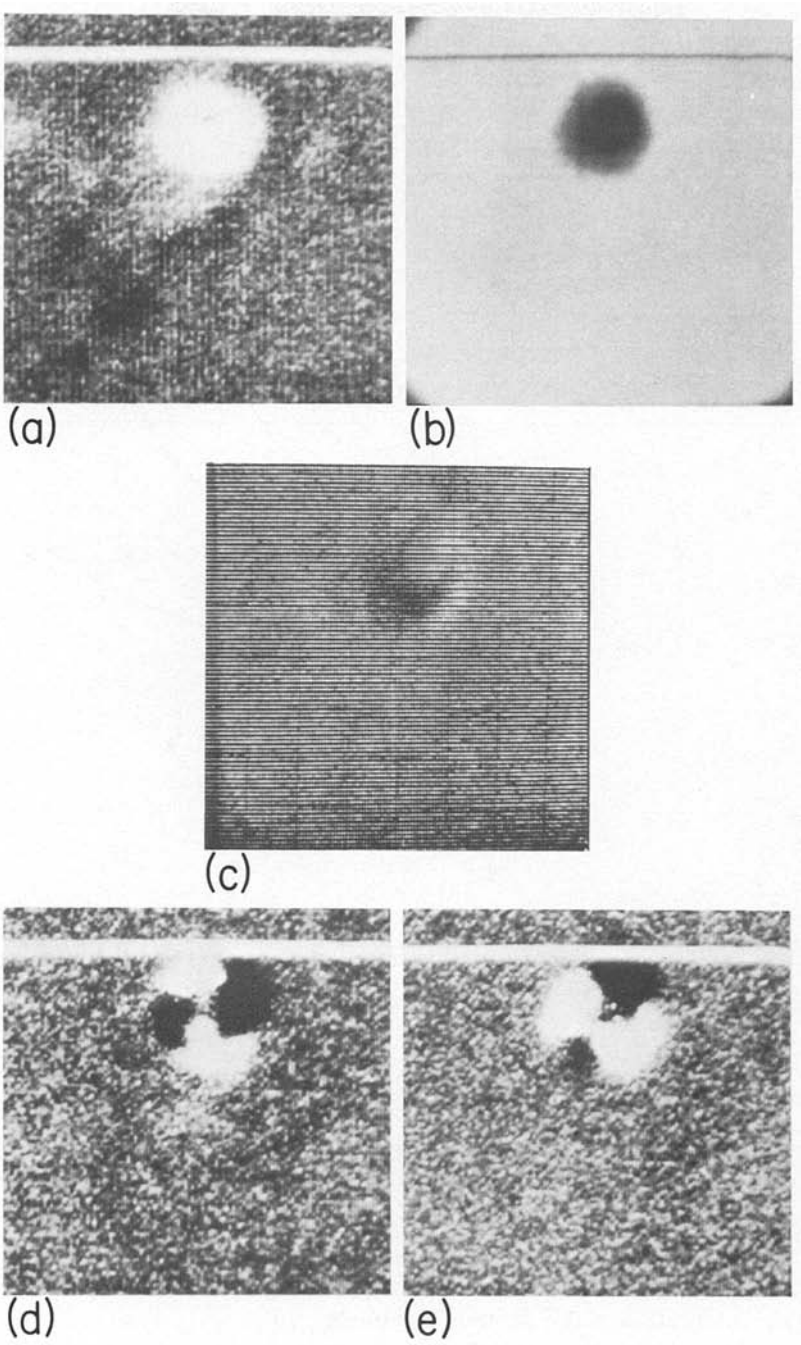

Fig. 1. Observational data for sunspot (Boulder Number 757) on 24 November 1976. (a) Net circularly polarized intensity distributions. (b) Corresponding picture of spot. (c) Net circularly polarized intensity distribution at line center. (d) Linearly polarized intensity distribution at 0°, 90° to analyzer. (e) Linearly polarized intensity distribution at 45°, 135° to analyzer.

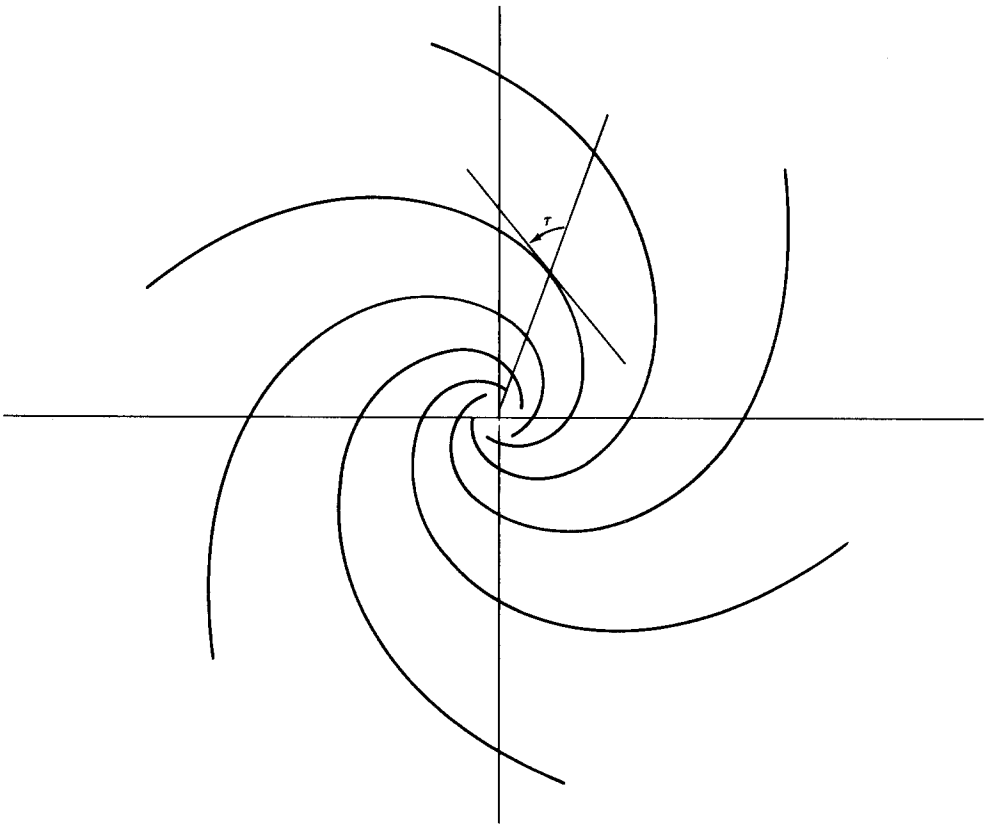

Fig. 2. The spiral angle τ.

actual measurements under this assumption that the transverse field strength (B_T) could be approximated by

$$B_T = (B_x^2 + B_y^2)^{1/2} \sim (P_Q)^{1/2}, \tag{1}$$

where P_Q is the measured degree of linear polarization. The azimuth angle ϕ ($\tan \phi = B_y/B_x$) was determined from the relative intensities of the linear polarizations in the two orientations (0° and 90°, 45°, and 135°) relative to the analyzer. The ambiguity of 180° in the azimuth ϕ was circumvented by making the *a priori* assumption that the transverse field was everywhere directed outwards from the umbra of the sunspot. The actual field lines were then calculated by numerical integration of the defining equations

$$\frac{dx}{B_x} = \frac{dy}{B_y} = \frac{ds}{B_T}. \tag{2}$$

The initial points in the calculation were chosen around the outer portion of the

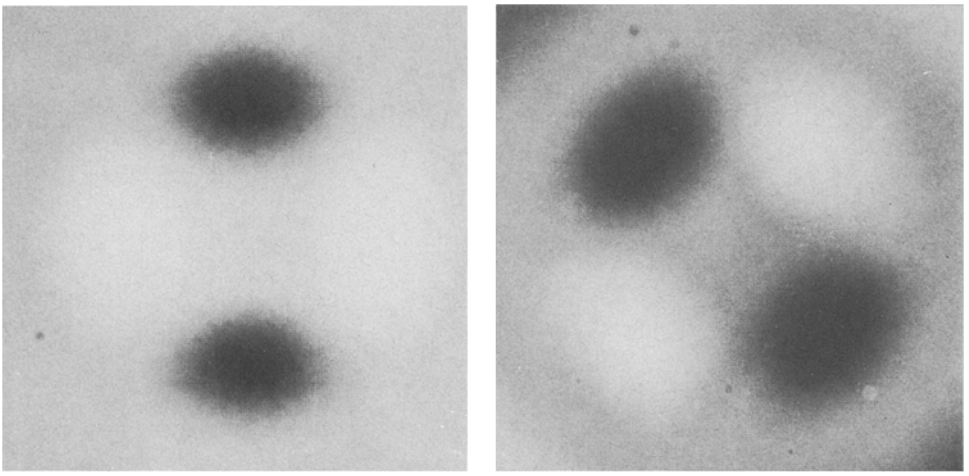

Fig. 3. Simulated linear polarization distributions; analyzer is oriented in horizontal direction. (a) Linearly polarized intensities at 0° and 90° to analyzer. (b) Linearly polarized intensities at 45° and 135° to analyzer.

umbra where the linearly polarized intensities begin to increase above the background level (see Figures 1d and 1e). The results of the calculation are shown in Figure 4, in which the calculated field lines are shown superimposed on a high-resolution Big Bear Solar Observatory Hα photograph which was taken 1 hr after the magnetic field data were obtained. In examining the results we attribute the small scale irregularities in the field lines to the noise-level variations in the unsmoothed transverse data. The large-scale patterns of the field lines appear consistent with a radial (potential) field with the exception of the field lines in the upper portion of the sunspot which display definite curvatures throughout their extent. Upon examination of a 4-day series of high-resolution Hα photographs from Big Bear Solar Observatory, in which the twisting of the Hα fibril patterns exhibits a definite relaxation over the period 22–25 November, it was determined that all the observational data clearly indicate a potential field distribution for this sunspot.

3. Theoretical Potential Field Calculation

In order to compare the observed transverse field configuration of this sunspot with a theoretical potential calculation, we used the representation of Teuber *et al.* (1977) in which the potential function is a solution of the Laplace equation for a semi-infinite rectangular volume with Neumann boundary conditions (Morse and Feshbach, 1953). In this method the measured longitudinal magnetic field data are

Fig. 4. Calculated transverse field lines and Hα photograph. (Hα photograph courtesy of Big Bear Solar Observatory.)

taken as the Z component of the potential field at the $Z = 0$ level and are expanded as a two-dimensional even function. Using Fast Fourier Transform (FFT) the expansion coefficients of the potential function are calculated and the potential itself is derived from the adjusted transform via inverse FFT. Since the vector field **B** is derived from the gradient of the potential, the transverse field strength at any level Z in the rectangular volume can be calculated. In Figure 5, the theoretical transverse field intensity at the $Z = 0$ level (b) is shown together with the observed transverse field distribution (a) which was calculated from the measured degree of linear polarization using Equation (1).

4. Comparison of Results

In comparing the observed and calculated transverse field intensities in Figure 5, there are obvious areas of agreement and disagreement. Both distributions exhibit the decrease in B_T near the central part of the umbra (although this feature is more pronounced in the observational data), and there is a qualitative similarity in the loci of regions of greatest intensity. Moreover, there is good quantitative agreement

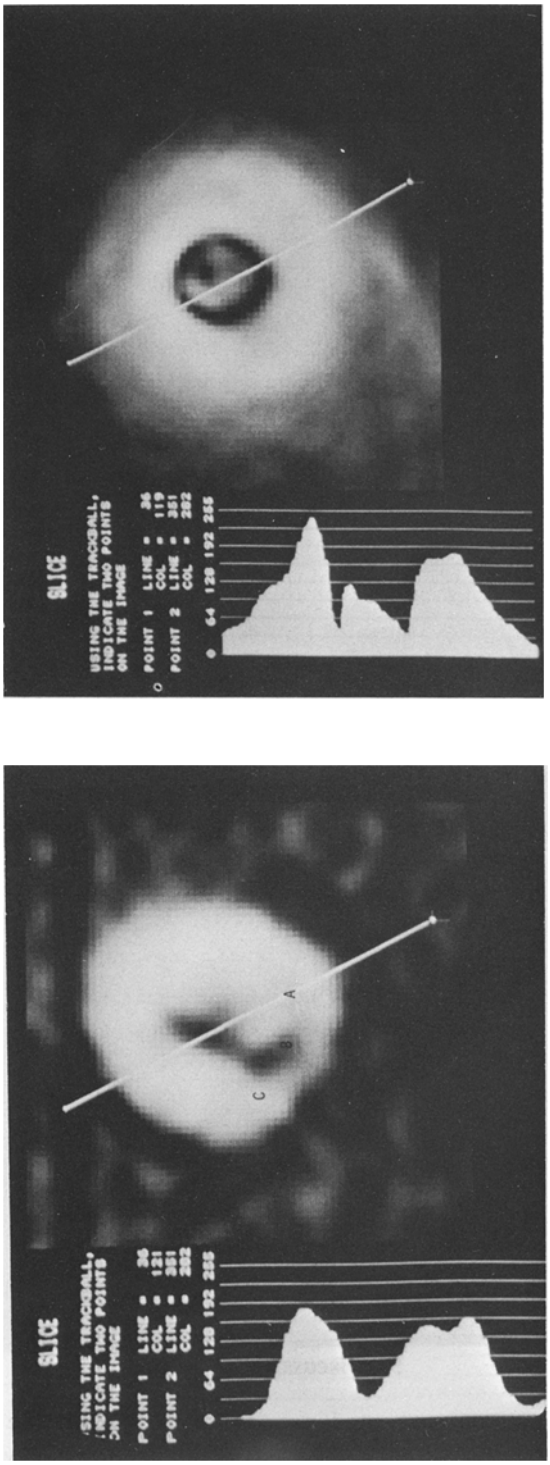

Fig. 5. Observed and calculated transverse field intensity. (a) Observations. (b) Potential theory calculation.

between the observed and calculated polarized intensities. As an example, the maximum measured degree of circular polarization is 6.04% [equivalent to a longitudinal field strength of 780 G based on calibrations using the Kjeldseth Moe and Maltby (1969) penumbral model]. With the input longitudinal field strengths scaled to this value, the calculated potential intensity (transverse) has a maximum value of 6.90% as compared to the measured maximum degree of linear polarization of 7.05%. Moreover, the calculated and measured maxima are co-located within an area of 4×4 arc sec.

The greatest disparity apparent in the comparisons of Figure 5 is the drop in the observed intensity (a) in the lower left (East) part of the penumbra of the sunspot. Specifically, in the regions marked *A*, *B*, and *C* in Figure 5a, the average measured degrees of linear polarization (P_Q) are 3.02%, 1.52%, and 3.28%, respectively. In the data analysis leading to the measured distributions of Figure 5a, the penumbral model of Kjeldseth Moe and Maltby (1969) was used in the calibration of the measured polarization signals throughout the field of view. However, as seen in Figure 4, the area (*B*) of reduced intensity corresponds to the region underlying the plage in the Hα photograph for 24 November. Thus it is quite likely that the drop in signal in area *B* is a consequence of the temperature sensitivity of the Fe I 5250.22 spectral line and does not represent a true decrease in field strength. In fact, comparisons of the inferred transverse fields based on the assumed penumbral model and on the plage model of Stenflo (1975) corroborate this conclusion, as shown in Table I. Actually, calibrations for the area *B* using the plage model probably over-correct for the temperature sensitivity; a value between 330 and 750 G would be more reasonable.

In any case, if allowances are made for the varying physical conditions throughout the active region in the data analysis, it seems clear that this particular discrepancy between the measured and calculated fields of Figure 5 would not be present.

TABLE I

Magnetic field dependence on atmospheric model

Region	Measured P_Q(%)	B_T (gauss)	
		Penumbral model	Plage model
A	3.02	480	–
B	1.52	330	750
C	3.28	510	–
Maximum	7.05	840	–

5. Discussion

If we accept the arguments presented previously to explain the 'gap' in the measured penumbral transverse field, then the major inconsistency between the

observed and calculated potential fields is in the umbral region of the sunspot. Some of the differences can be attributed to noise in the observational data. However, a more physical explanation seems to be involved based on the interpretation of the longitudinal data and on the mathematical implications of potential theory. The input data for the potential calculation are the net circularly polarized intensities P_V. As curve *a* in Figure 6 indicates, P_V is directly proportional to the longitudinal magnetic field (B_L) for field strengths up to approximately 1000 G. For higher field strengths the circular polarization signal deviates from this linear relation, and beyond ≈3000 G P_V actually decreases with increasing field strength. Based on an examination of the circularly polarized intensities in the umbral region as shown in Figure 1a, it is evident that these intensities are decreasing in the upper (NW) part of the umbra. Since the longitudinal field is expected to be strongest in

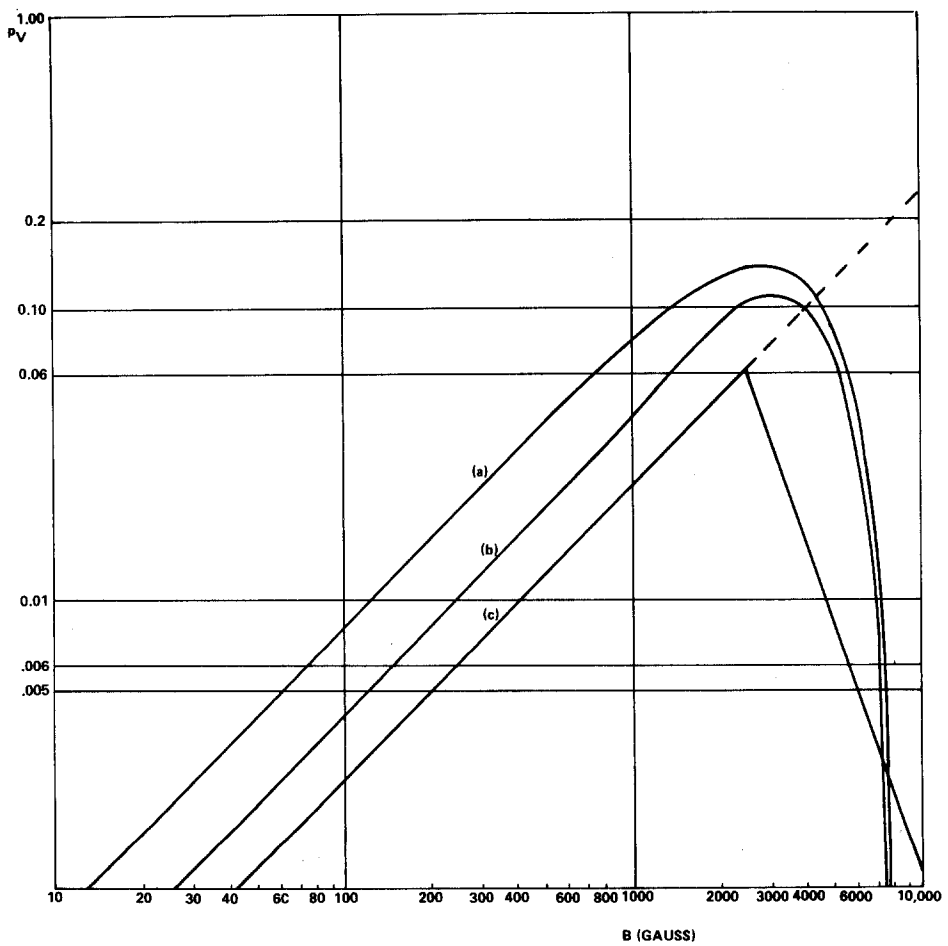

Fig. 6. Variation of net circular polarization P_V with magnetic field strength B for a penumbral model. (a) Longitudinal field case ($\psi = 0°$). (b) $\psi = 60°$. (c) Schematic calibration curve.

the umbra, it seems that the decreased P_V signal is indicative of very strong fields rather than the unusually weak fields which would be inferred from a linear relation between P_V and B_L. Thus by using the measured P_V distribution rather than the actual longitudinal field in the potential calculation, we force the potential function to compensate for these irregularities in the umbra in order that the potential at every point be equal to the spatial average of the potential at neighboring points as potential theory dictates. And we believe that it is this compensation of the potential function which produces the unusual transverse field structure seen in the umbral region of Figure 5b.

In order to test this conclusion we repeated the potential field calculation using as boundary conditions an inferred longitudinal field distribution rather than P_V. Since the observational data were not sufficient to exactly specify the very strong longitudinal field B_L, where

$$B_L = B \cos \psi ,$$

we employed the schematic calibration curve c in Figure 6 to infer the longitudinal fields from the diminished P_V values in the umbral region. The choice of this schematic curve is based on the following arguments. In order to obtain a continuous variation of B_L around the measured maximum value of P_V of 6.04% and to preserve this continuity as P_V drops from maximum down to the measured minimum of 0.50% in the umbra, it is necessary to have the theoretical calibration curve peak near 6%. As can be seen from curves a and b in Figure 6, no reasonable value of the field inclination ψ gives a maximum P_V near 6% for the penumbral model used. This problem very likely is indicative of the inadequacy of the theoretical interpretation used and of the chosen atmospheric model. [Umbral models suitable for the Fe I 5250.22 spectral line calculations are not available at the present time (see Dunn, 1972).] Thus we chose as the first branch of the schematic calibration a linear curve for which the maximum P_V of 6% corresponds to 2500 G (slightly less than the 3000 G maxima of the actual calibration curves). For the second branch, the minimum P_V of 0.5% was chosen to correspond to a field strength of 6000 G which, again, is less than the values of $\approx$7500 G given by curves a and b in Figure 6. The triangular shape was chosen so that the monotonically descending values of P_V (from 6% down to 0.5%) translate into a continuous increase in field strength (from 2500 up to 6000 G); a curve similar to a or b in Figure 6 would result in large field increments near the 6% maximum. Finally, we argue that this exercise is not to infer the actual longitudinal field of the umbra of region 757 but rather to indicate the effect of the proper interpretation of the circularly polarized signal P_V on a potential field calculation while maintaining the integrity of the data as much as possible. Therefore, the data from the umbral regions where the P_V signals were diminished were reinterpreted on the basis of 'calibration curve' c of Figure 6, and these recalibrated data were then used as boundary values in our potential theory calculation. Figure 7 shows the results of this recalculation of the potential transverse field at the $Z = 0$ level. In comparing these results with the measured

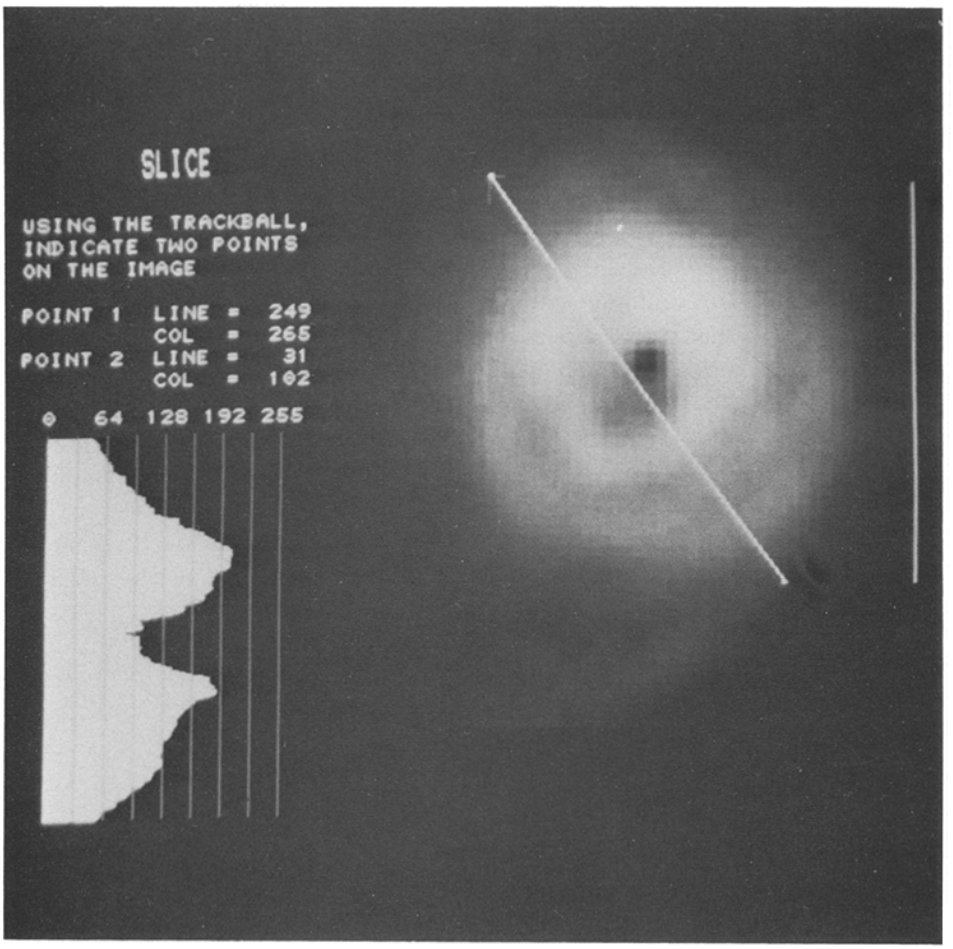

Fig. 7. Re-calculation of transverse field intensity from potential theory.

transverse field shown in Figure 5a we observe the excellent morphological agreement which has been achieved through this interpretation of the circular polarization in the umbra. Moreover, the new value of maximum linear polarization is 7.27%, which is still in good quantitative agreement with the measured value (7.05%).

In concluding this discussion, we should mention two further effects which might be important sources of discrepancy between the observed and calculated transverse fields. First, the transverse field was inferred from the measured linear polarization using Equation (1) which is valid within an accuracy of $\approx$50 G only for field strengths less than 500 G. Second, there is the unavoidable error in the determination of the transverse field from the spatially-averaged linear polarization

for highly localized (and therefore spatially unresolved) field strengths. For example, in the case of a localized flux tube with a transverse field of 300 G occupying an area of one-tenth the area of a resolution element, the spatially-averaged linear polarization translates into an average field value of ≈90 G rather than 30 G. This discrepancy is a consequence of the non-linear relation between the transverse field and the degree of linear polarization, and it is inherent in a polarimeter-type magnetograph. The good quantitative agreement found in the comparisons of this paper would indicate that the transverse fields for this active region were not highly localized within the resolution element of 1.3×1.3 arc sec.

In conclusion, this study implies that if we take as input to the theoretical calculation the measured longitudinal field B_L, including saturation effects and assume Neumann boundary conditions, then the computed transverse potential field will represent closely the measured transverse field, provided that the measured linear polarization P_Q is interpreted on the basis of appropriate atmospheric conditions. The implication of this for potential field extrapolations from photospheric longitudinal data is that a correct potential field representation depends in a sensitive manner on the proper interpretation of the measured circularly polarized intensities.

References

Altschuler, M. D. and Newkirk, G., Jr.: 1969, *Solar Phys.* **9**, 131.
Dunn, A. R.: 1972, *Solar Phys.* **26**, 83.
Hagyard, M. J., West, E. A., and Cumings, N. P.: 1977, *Solar Phys.* **53**, 3.
Kjeldseth Moe, O. and Maltby, P.: 1969, *Solar Phys.* **8**, 275.
Morse, P. M. and Feshbach, H.: 1953, *Methods of Theoretical Physics*, Part II, McGraw-Hill Book Company, Inc., New York.
Schmidt, H. U.: 1964, in W. N. Hess (ed.), *Physics of Solar Flares*, NASA SP-50.
Stenflo, J. O.: 1975, *Solar Phys.* **42**, 69.
Teuber, D., Tandberg-Hanssen, E., and Hagyard, M. J.: 1977, *Solar Phys.* **53**, 97.